J. Fluid Mech. (1988), *vol.* 194, *pp.* 233–259
Printed in Great Britain

Baroclinic instability of three-layer flows Part 2. Experiments with eddies

By DAVID A. SMEED

Department of Applied Mathematics and Theoretical Physics, University of Cambridge, Silver Street, Cambridge CB3 9EW, UK

(Received 8 April 1987 and in revised form 26 January 1988)

The stability of eddies with three-layer stratification is examined experimentally. When the difference in density between the upper two layers is much greater (or less) than that between the lower two layers baroclinic instability on two different lengthscales (the Rossby radii associated with the upper and the lower interfaces) is possible. The vortices are created using modifications of two techniques described by Griffiths & Linden (1981) in their study of two-layer eddies.

'Constant-flux' eddies are generated by the release of a constant flux of buoyant fluid from a small source positioned at the surface of a two-layer fluid. In a second variation of this experiment, the source is positioned at the interface between two layers and fluid of intermediate density is injected. As the horizontal lengthscale increases, the vortices evolve from a stable to an unstable state. It is showns that the size at which the vortices become unstable may be significantly altered by the presence of a second interface. The results agree qualitatively with the conclusions of a linear stability analysis of quasi-geostrophic three-layer flow in a channel (Smeed 1988), but it is necessary to examine the effects of horizontal shear and Ekman dissipation to explain the experimental results.

'Constant-volume' eddies are produced by the release of a volume of buoyant fluid, initially contained within a cylindrical barrier, at the surface of a two-layer fluid. After the barrier is removed, the buoyant fluid spreads a distance of the order of the Rossby radius. Similarly, vortices are created by releasing a volume of fluid of density intermediate between the initial two layers. Within a few rotation periods the vortices become unstable to disturbances similar to those observed in two-layer experiments. Qualitative agreement is found between the observed wavelength and the fastest growing mode predicted by the linear stability theory (Smeed 1988). When the disturbances reach large amplitude a change in lengthscale is often observed.

1. Introduction

A number of experimental studies of instability in two-layer stratified, rotating fluids have been described, e.g. Hart (1972), Saunders (1973), Griffiths & Linden (1981*a*, *b*, 1982) and Griffiths, Killworth & Stern (1982). Such flows, with their simple vertical structure, have been successful in elucidating many features of instability observed in more complex flows. There are, however, some problems that cannot be addressed using two-layer models. In particular, what is the effect of non-uniform stratification? This question was addressed in an accompanying paper (Smeed 1988, hereinafter referred to as S1) by examining the linear stability of three-

layer flow in a channel. The study is continued in this paper, in which experiments with eddies in three-layer stratified, rotating fluids are discussed.

Warm eddies in the oceans are often characterized by a layer of almost homogeneous water above a strong pycnocline. They are often observed to be elliptical in shape with arms of warm water spiralling out from the centre (e.g. Evans *et al.* 1985; Griffiths & Pearce 1985). Similar features have been observed in unstable two-layer vortices in experiments described by Griffiths & Linden (1981*a*), (hereafter referred to as GL). Griffiths & Pearce (1985) suggested that instabilities similar to those reported by GL are responsible for the deformation and breakup of warm eddies. Although two-layer vortices model many of the essential features of warm eddies, they cannot include the effect of stratification below the main pycnocline. Such stratification will change the vertical structure of unstable perturbations and may be important in determining the conditions required for stability. The simplest representation of stratification below the pycnocline is the addition of a second interface, and it is proposed that the experiments described here, with three-layer vortices, model some features of warm eddies with stratification below the pycnocline. As in S1, attention is focused on the case in which the change in density across one interface is much greater than the change in density across the other interface. The qualitative results are though pertinent to other flows with non-uniform stratification. It was noted in S1 that three-layer flows can model qualitatively the first three normal modes of continuously stratified flows but that the analogy between the two problems is not an exact one.

The analysis described in S1 was of a quasi-geostrophic flow in a channel similar to the two-layer model of Phillips (1954). The case in which the difference in density between the lower two layers was much less than that between the upper two layers was examined. The range of unstable wavenumbers was found to be dependent upon S, the ratio of the slope of the lower interface to the slope of the upper interface. Short-wavelength instabilities associated with the lower interface were found to grow only when $|S| > 1$. The fastest growing modes were those associated with the lower interface only when $|S| \gtrsim \epsilon^{-\frac{1}{2}}$, where ϵ is the ratio of the density difference across the lower interface to that across the upper interface.

Two methods of generating anticyclonic eddies are used in the experiments. Both of these were first described by GL in their study of the stability of two-layer stratified vortices. The stability of two-layer vortices has been examined further by Smeed (1986). These techniques have been adapted to examine the behaviour of three-layer vortices. The axisymmetric behaviour prior to instability is discussed in §§3 and 4. In §§5 and 6 the critical conditions for instability and the initial mode of instability are compared with the results of the quasi-geostrophic analysis, and large-amplitude features of the perturbations are described.

In the first series of experiments described by GL, a volume of buoyant fluid, initially contained within a cylindrical barrier, is released at the surface of a homogeneous rotating fluid layer. These will be referred to as 'constant-volume' experiments. When the barrier is removed, the buoyant fluid spreads radially outwards, generating anticyclonic motion in the upper layer. At the same time cyclonic motion is generated in the lower layer, as lower-layer fluid moves radially inwards. Within a time $O(f^{-1})$ (f is the Coriolis parameter) the spreading of the surface front is halted as the horizontal pressure gradients are balanced by the Coriolis and centrifugal forces arising from the azimuthal motion. Disturbances with azimuthal wavenumber $N \geqslant 2$ become apparent within 2 or 3 rotation periods. Similar experiments, in which negatively buoyant fluid initially contained within a

cylindrical barrier extending through the total depth of fluid was used, were described by Saunders (1973).

To interpret their observations GL used the simple model of two-layer flow in a channel first described by Phillips (1954). In this model, the flow is assumed to be quasi-geostrophic and uniform within each layer. The experimental flows had, though, horizontal shear of the velocity and significant non-quasi-geostrophic aspects. In particular the upper layer was bounded by a front at which the interface intersected the upper surface and the Rossby number was $O(1)$. Despite these differences, good agreement was found between model and experiments. GL concluded that, when the depth ratio $\delta \gtrsim 0.2$ (δ = initial upper layer depth H_1/total depth of fluid H), the instabilities were primarily baroclinic.

The stability of a surface front in a two-layer geostrophic flow has been examined numerically by Killworth, Paldor & Stern (1984). Killworth *et al.* found that the fastest growing modes had wavelengths very similar to those predicted by Phillips' (1954) model. Non-dispersive long-wave frontal instabilities were also found, but these had smaller growth rates. Other experimental studies of the stability of two-layer flows with surface fronts (Chia, Griffiths & Linden 1982; Griffiths & Linden 1982; Griffiths *et al.* 1982) have also been in good agreement with Killworth *et al.*'s and Phillips' (1954) calculations. The success of the Phillips model in explaining the results of these studies suggested that the experiments described here could illustrate, and be interpreted by, the results of the quasi-geostrophic analysis in S1.

GL also described 'constant-flux' experiments, in which buoyant fluid is released continuously from a small source at the surface of a homogeneous rotating fluid, or in the interior of a linear stratification. As the buoyant fluid spreads, anticyclonic motion (in the rotating frame of reference) is generated in the upper layer. If the fluid were inviscid it would conserve its angular momentum, so that the azimuthal velocity in the upper layer would be $-\frac{1}{2}fr$ (r is the radial coordinate), for a point source. It is, however, modified by dissipation. The resulting profile has a peak value at a radius of the order of $R_\nu = (Q/\pi)^{\frac{1}{2}}(\frac{1}{8}f\nu)^{-\frac{1}{4}}$, where Q is the volume flux, and ν is the kinematic viscosity (Gill *et al.* 1979; GL; Smeed 1986). Anticyclonic motion is also generated in the lower layer, both by squashing as the upper layer deepens and spin-down due to the interfacial Ekman layer, but it is also spun-up by the bottom Ekman layer. A velocity profile similar to that of the upper layer is thus produced. GL observed that the surface eddies grew in size until they reached a critical radius at which the Froude number

$$\gamma = \frac{f^2 R^2}{g' H[\delta(1-\delta)]^{\frac{1}{2}}} \tag{1}$$

(where R is the radius of the vortex, and g' is the reduced gravity) exceeded a critical value γ^* and the eddies became baroclinically unstable. The measured values of γ^* were in the range $10 \lesssim \gamma^* \lesssim 100$, significantly greater than would be expected from simple baroclinic theory. Smeed (1986) proposed that the variation in γ^* was due to the gradient of relative vorticity which is such as to reduce the gradient of potential vorticity in the lower layer, thus stabilizing the vortices. When the injection of upper-layer fluid starts, the potential vorticity in the lower layer is uniform, and if the fluid were inviscid the potential vorticity would remain uniform. In this case we would expect (according to quasi-geostrophic theory) the vortex to remain stable. However, Ekman pumping reduces the anticyclonic vorticity in the lower layer allowing a gradient of potential vorticity to form, and eventually the vortex becomes

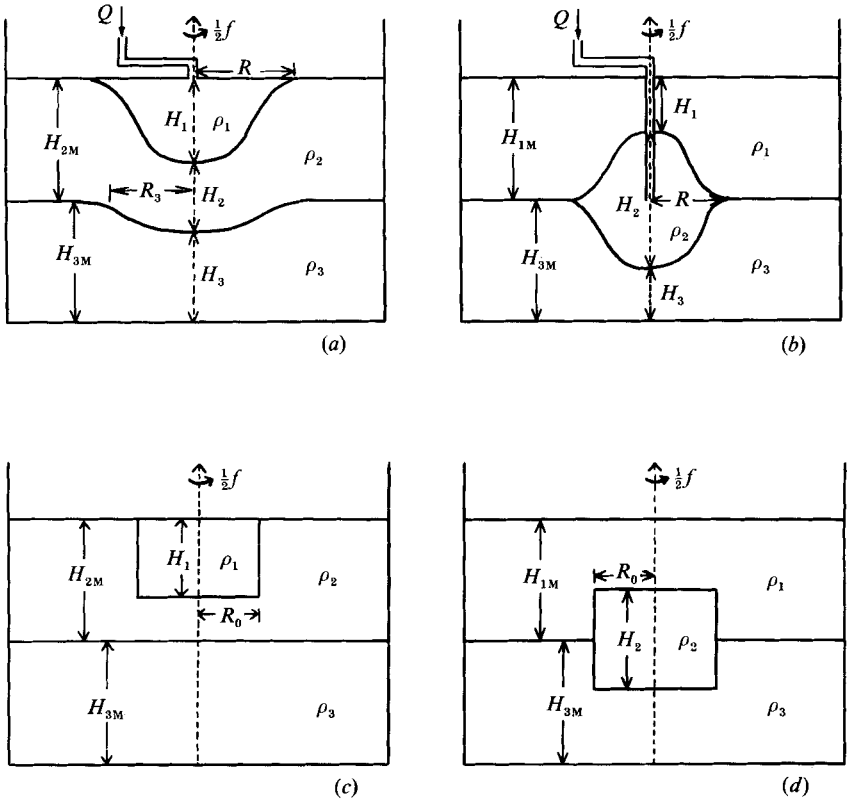

FIGURE 1. Three-layer eddies. (*a*) Surface-flux experiments. (*b*) Intermediate-flux experiments. (*c*) Surface-volume experiments. (*d*) Intermediate-volume experiments. In each experiment there is a three-layer stratification in $r < R$ and two-layer stratification in $r > R$. The ith layer has depth H_i at $r = 0$, maximum depth H_{iM}, and density ρ_i. The initial radius of the constant-volume eddies (*c* and *d*) is R_0. The radius of the sloping region of the lower interface in the surface-flux experiments (*a*) is R_3.

unstable. Smeed (1986) showed that γ^* was correlated to λ, a measure of the mean vertical shear across the interface relative to the horizontal shear in the lower layer:

$$\lambda = \left(\frac{g'H_1}{fR}\right) \Big/ \tfrac{1}{2}fR. \tag{2}$$

Smeed (1986) remarked further that the interface slope at the surface front was small and that the front did not appear to be important in the growth of instabilities. Thus, rather than the radius of the front a better measure of the radius of the eddy was

$$R = \left(\frac{2V}{\pi H_1}\right)^{\frac{1}{2}}. \tag{3}$$

$V = Qt$ is the volume of the upper layer (t is the time elapsed since the beginning of the experiment). This definition of R will be used when calculating γ (equation (1)) in this paper.

Two extensions of the constant-flux experiments have been examined. In the first

(figure 1*a*) a constant flux of buoyant fluid was released at the surface of two-layer stratified rotating fluid. In the second variation, fluid of density intermediate between that of the upper and lower layers of a two-layer stratified fluid was introduced at the interface between the initial two layers (figure 1*b*). These will be referred to as 'surface-flux' and 'intermediate-flux' experiments.

The constant-volume experiments were modified in similar ways. In the 'surface-volume' experiments (figure 1*c*), a volume of buoyant fluid was released at the surface of a two-layer stratified rotating fluid, by removing a cylindrical barrier (radius R_0) within which the buoyant fluid was initially confined. Eddies were also produced by releasing fluid, initially contained within a cylindrical barrier, of density intermediate between that of the upper and lower layers (figure 1*d*); these will be referred to as 'intermediate-volume' experiments.

2. Experimental procedures and methods of visualization

The experiments were conducted in one of two cylindrical tanks; one 89.2 cm in diameter and 30 cm deep, the other 74 cm in diameter and 44 cm deep. The apparatus was mounted on a rotating table of angular velocity $\frac{1}{2}f$ (0.25 rad s^{-1} $< f <$ 2.5 rad s^{-1}). In both sets of experiments, three different densities of fluid ($\rho_1 < \rho_2 < \rho_3$) were used (figure 1). g_1', g_2' are, respectively, the reduced gravity at the upper and lower interface (0.2 cm s^{-2} $< g_1', g_2' <$ 20 cm s^{-2}):

$$g_i = 2g\left(\frac{\rho_{i+1}-\rho_i}{\rho_i+\rho_{i+1}}\right).$$

The density contrasts were obtained by the addition of salt to fresh water. All measurements were taken from still photographs or video recordings taken by cameras mounted on the rotating table.

'*Surface-flux*' *experiments.* These experiments were carried out in a manner identical to that described in by GL, except that the source of buoyant fluid was positioned at the surface of a two-layer stratified flow instead of a homogeneous layer. The buoyant fluid was introduced through a brass tube, outer diameter 0.6 cm, the lower end of which was covered by a piece of foam rubber roughly 1.5 cm in diameter. The height of the 'source' was adjusted so that the foam rubber protruded 0.2 cm below the water surface. The axis of the cylindrical tank and the brass tube were vertical and coincident with the axis of rotation (to within 0.1 cm). The tank was covered with a Perspex lid, but there was always a gap of several centimeters between the water surface and the lid. Thus the upper surface was, as far as was possible, stress free. The volume flux of buoyant fluid was monitored by a flow meter. In some experiments the flux was observed to change by up to 10%, but these changes occurred on a timescale of the order of the length of the experiment (O(10 min)). The analysis in S1 indicated that a method of visualization was required that would enable all three layer depths to be observed during an experiment. For this reason, the flow was visualized by dyeing the upper and lower layers with flourescein. A plane of light, approximately 0.5 cm thick, illuminated a vertical section passing through the axis of rotation. Photographs were taken from the side.

'*Intermediate-flux*' *experiments.* In these experiments the brass tube extended through the depth of the upper layer, so that the source was positioned at the interface between the initial two layers. The flow was visualized by colouring the

source fluid (i.e. the middle layer) with a dark dye. Photographs were taken from the side.

'Surface-volume' experiments. These were undertaken in a similar way to the experiments described by GL, except that the homogeneous lower layer was replaced by a two-layer stratified fluid. The presence of the lower interface meant that the buoyant fluid within the cylindrical barrier had to be added at a rate sufficiently slow to minimize the motion generated (by squashing) in the middle layer which was not in contact with a rigid boundary and thus only spun-up by interfacial friction. The buoyant fluid within the cylindrical barrier was added at the same time as the lower layer. These experiments were visualized by dyeing the buoyant fluid a dark colour and observing the experiments in planform.

'Intermediate-volume' experiments. In these experiments the cylindrical barrier extended to the bottom of the tank. To set up the flow the upper layer was first allowed to spin-up. Then, outside the barrier, the lower layer was added through a ring with a large number of small holes around the bottom of the cylindrical wall of the tank. Inside the barrier, the middle layer was first added through a small source on the bottom of the taken before the lower layer was added through a second source on the tank bottom. A rubber seal was used to prevent flow under the barrier and care was taken to keep the total depth of fluid on either side as close as possible during the filling procedure. The flow was visualized by dyeing the middle layer, and the experiments were viewed in planform.

3. Axisymmetric behaviour of constant-flux vortices

Smeed (1986) showed that the two-layer eddies evolve through a continuous series of quasi-cyclostrophic states. The evolution is determined by the squashing and stretching of vortex lines within each layer, due both to the changes in height of the interface and Ekman pumping by the interfacial and bottom boundary layers. The same processes determine the evolution of three-layer eddies, but are modified by the presence of the second interface. Because of the long time required to set up the stratification, the lower interface is thicker than the Ekman-layer depth $(2\nu/f)^{\frac{1}{2}}$, whereas the upper interface thickness is of the order of the Ekman-layer depth. Thus the lower interface is less significant to the spin-down process than is the upper interface.

Once the experiment has begun, anticyclonic motion is generated in the upper layer as the buoyant fluid spreads outwards and anticyclonic motion is induced in the middle layer, owing both to squashing as the upper layer deepens and spin-down by the upper interface. The lower interface is also depressed, causing anticyclonic motion in the lower layer too. This is opposed by spin-up by the bottom Ekman layer.

An example of a three-layer vortex is shown in figure 2. In this case $\epsilon = g_1'/g_2' = 0.25$. The slope of the lower interface is greater than that of the upper interface (figure 2*a*). This feature was observed in all experiments with $\epsilon < 1$ (except during the first few rotation periods of each experiment) and demonstrates the importance of the upper interfacial Ekman layer, since if the fluids were inviscid the lower interface would always be depressed less than the upper interface. (If the lower interface was depressed *more* than the upper interface and potential vorticity was conserved, there would be a cyclonic circulation in the middle layer and anticyclonic motion in the bottom layer – but this would imply that the lower interface slopes downwards (as r increases).) In some of the experiments in which $\epsilon < 1$ the

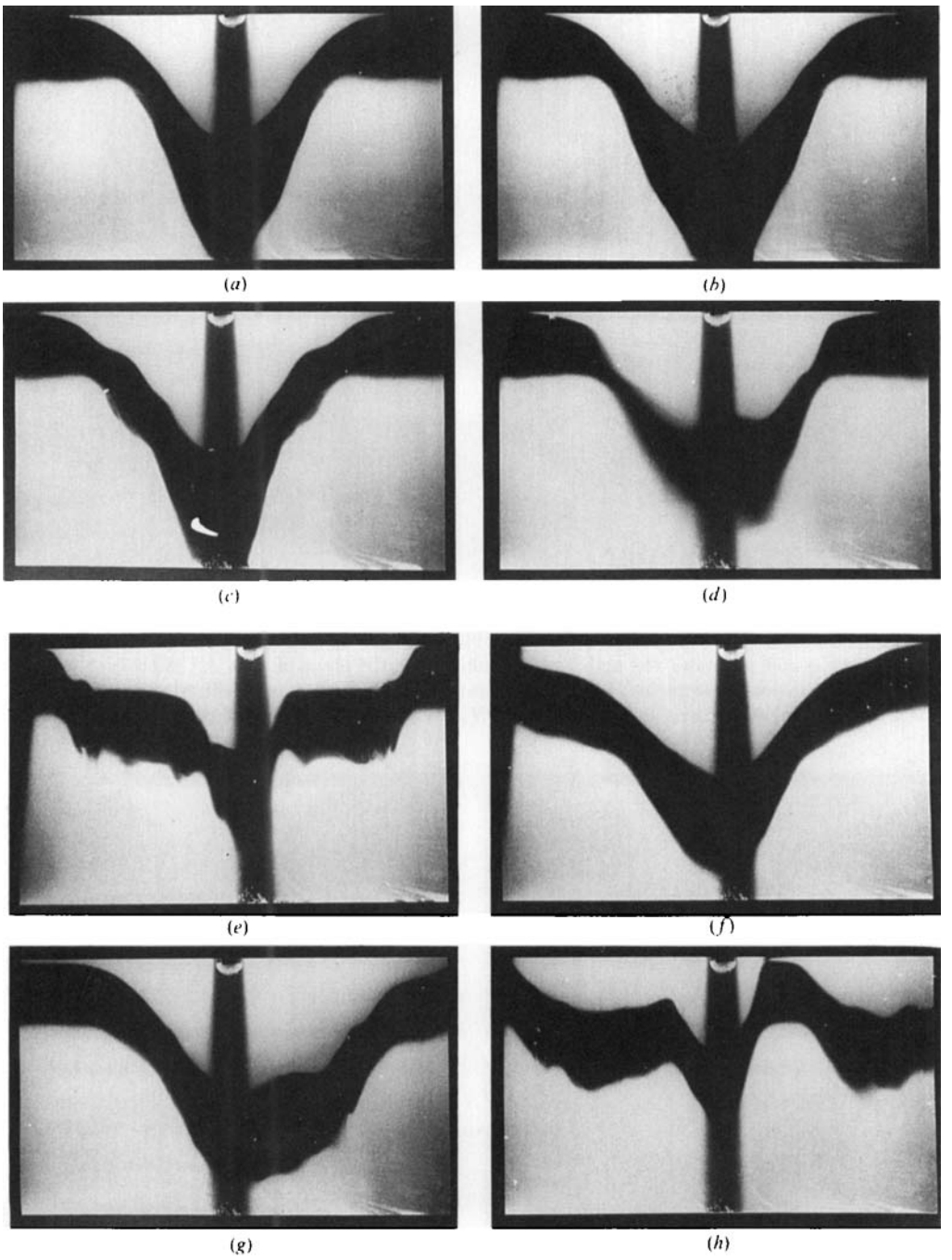

FIGURE 2. 'Surface-flux experiment', $\epsilon = 0.25$. A vertical slice is visualized using the slit-lighting technique (see text). The upper and lower layers were dyed with flourescein and appear white in the photographs. The dark vertical band in the centre of the photographs is a shadow due to the source used to introduce the buoyant fluid. (*a*) 157 revs: the eddy is stable. (*b*) 209 revs: the first signs of an $N = 2$ instability can be seen. (*c*) 215 revs: the amplitude has increased. (*d*) 222 revs: the core of the vortex is now elliptical, the major axis of which is in the plane of view. (*e*) 244 revs: the minor axis of the elliptical core is in view. (*f*) 288 revs: the eddy has restabilized. (*g*) 316 revs: a second instability has developed. (*h*) 330 revs: the instability has reached large amplitude and the vortex is splitting. $f = 2.17$ rad s^{-1}; $g_1' = 1.0$ cm s^{-2}; $g_2' = 0.25$ cm s^{-2}; $H_{2M} = 5.0$ cm; $H_{3M} = 15.0$ cm; and $Q = 1.35$ cm^3 s^{-1}.

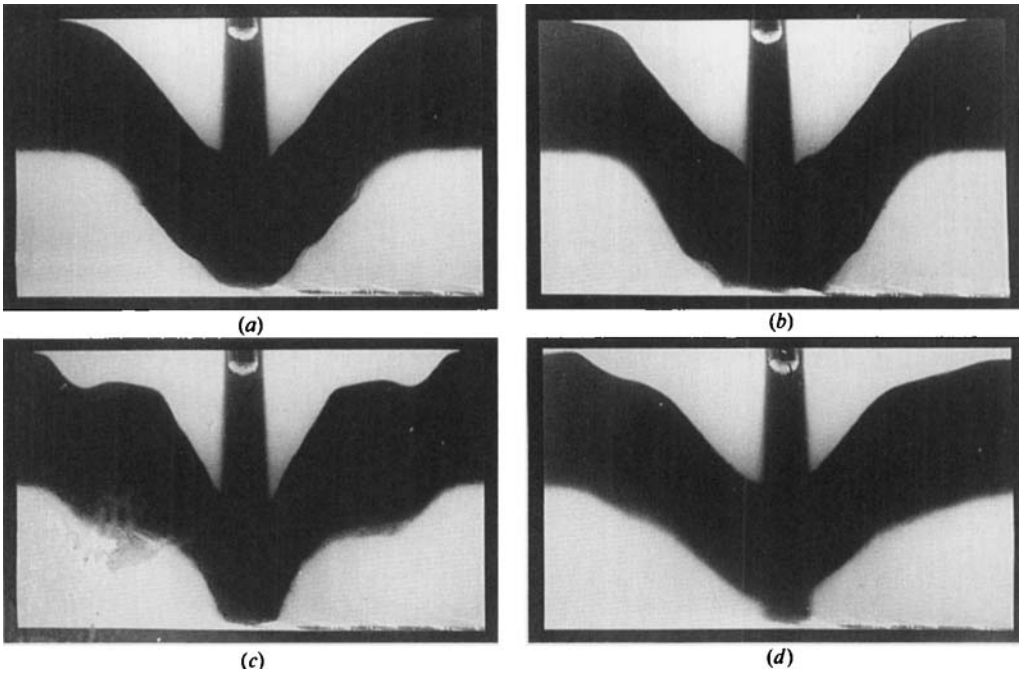

FIGURE 3. 'Surface-flux experiment', $\epsilon = 1$. (*a*) 149 revs: the eddy is stable. (*b*) 181 revs: the core of the vortex is now elliptical, the major axis of which is in the plane of view. (*c*) 183 revs: the minor axis of the elliptical core is in view. (*d*) 209 revs: the eddy has restabilized. $f = 2.14$ rad s^{-1}; $g_1' = 1.0$ cm s^{-2}; $g_2' = 1.0$ cm s^{-2}; $H_{2M} = 9.5$ cm; $H_{3M} = 9.5$ cm and $Q = 1.45$ cm^3 s^{-1}.

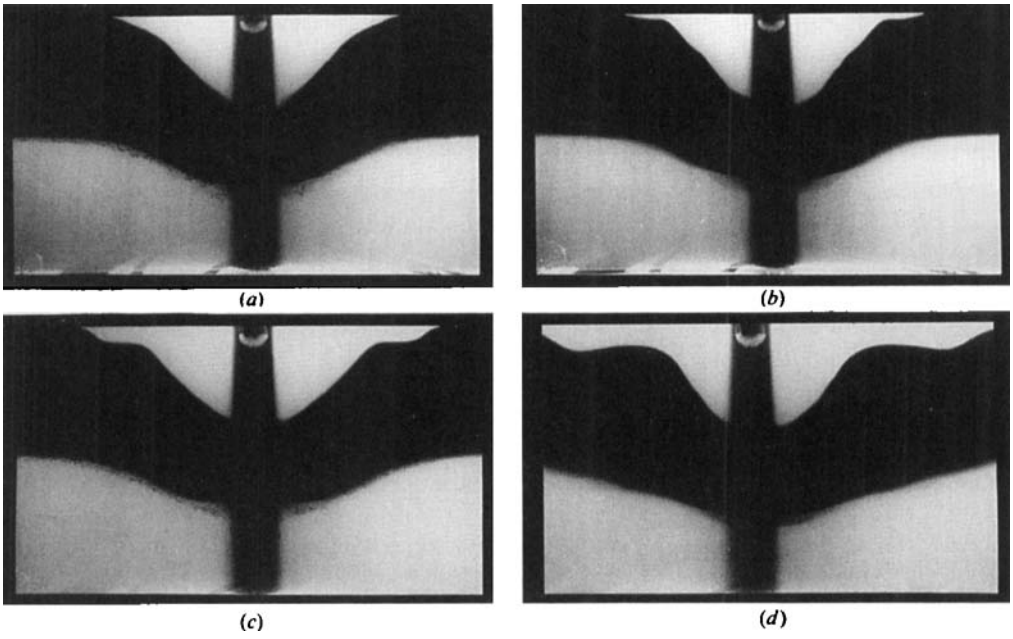

FIGURE 4. 'Surface-flux experiment', $\epsilon = 5.0$. (*a*) 81 revs: the first signs of instability can be seen. (*b*) 89 revs. (*c*) 103 revs. (*d*) 164 revs: the eddy has restabilized but a second disturbance is now apparent. $f = 2.14$ rad s^{-1}; $g_1' = 1.0$ cm s^{-2}; $g_3' = 5.0$ cm s^{-2}; $H_{2M} = 9.5$ cm; $H_{3M} = 9.5$ cm and $Q = 1.25$ cm$^{3\,s^{-1}}$.

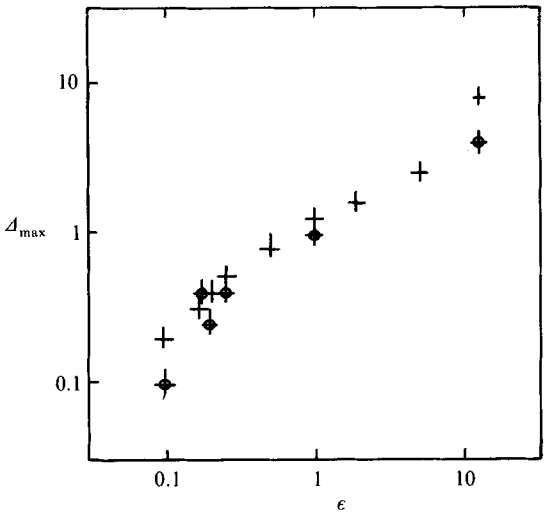

FIGURE 5. The maximum value $\Delta_{\max}$ of Δ *vs.* ϵ for the surface-flux experiments. Experiments in which bottom or interfacial fronts were formed are indicated by circles (○). $\Delta = g_2'(H_{3M}-H_3)/g_1'H_1$.

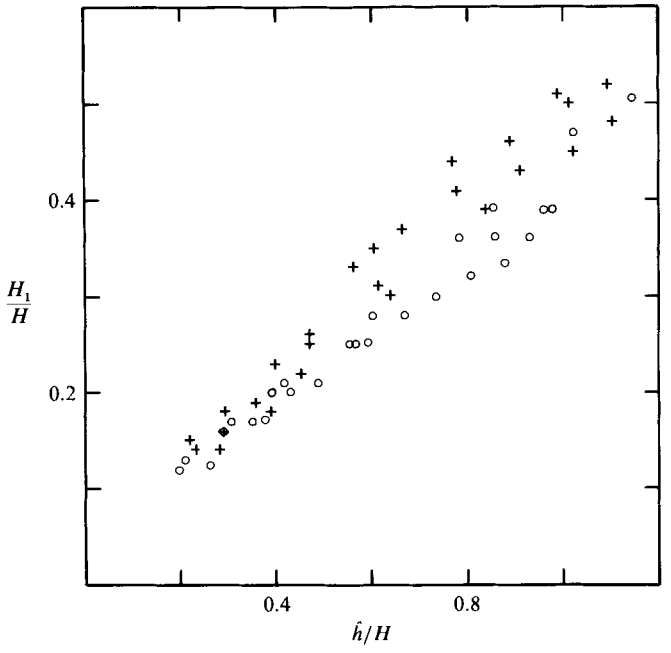

FIGURE 6. The measured depth fraction H_1/H *vs.* $\hat{h}/H$ calculated by the inviscid theory of GL for a two-layer vortex. The parameters were the same in each experiment except for g_2' and $H_{2M}/H_{3M}(H_{2M}+H_{3M}$ was kept constant). 0, $\epsilon \geqslant 0.5$; +, $\epsilon < 0.5$.

lower interface, after some time, intersected the bottom boundary forming a front (figure 2*b*), similar to those examined in experiments on bottom fronts by Smeed (1987). The observations show that the width of the region over which the lower interface slopes is a little less than the radius R of the upper layer. A second lengthscale R_3 of the eddy may then be defined as the radius at which the depth of the lower layer came within (say) 5% of its undisturbed value (see figure 1).

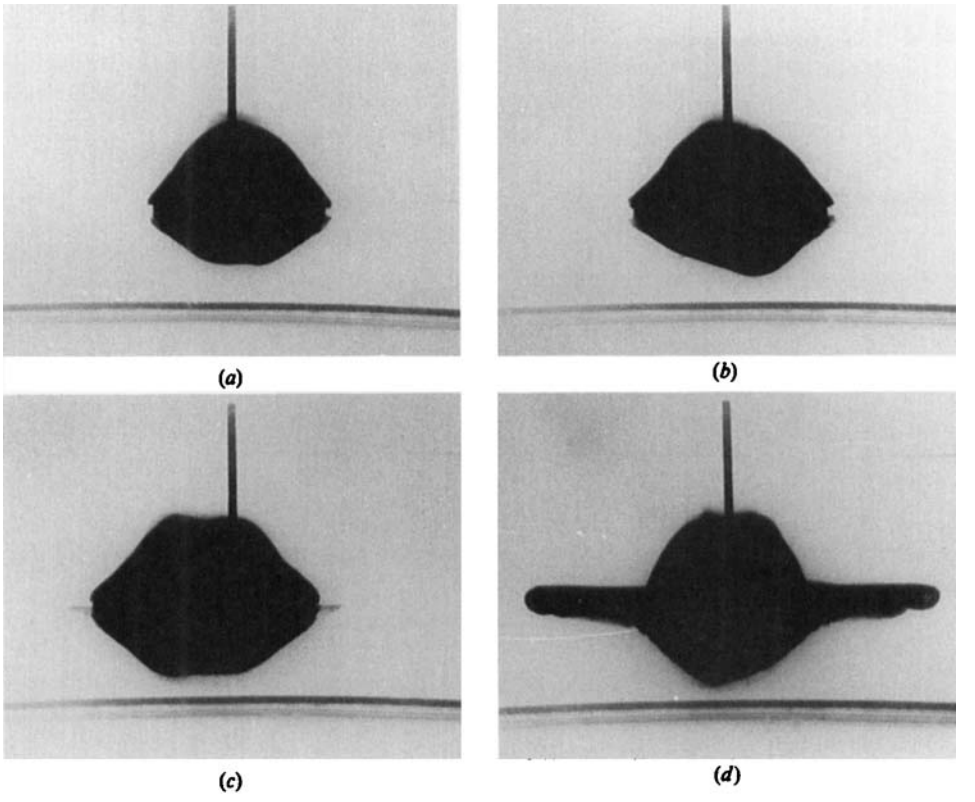

FIGURE 7. 'Intermediate-flux experiment', $\epsilon = 0.91$. (*a*) 41 revs: the vortex is stable. (*b*) 52 revs: a perturbation with $N = 1$. (*c*) 75 revs: an $N = 2$ disturbance is also apparent. (*d*) 94 revs: the $N = 2$ instability has reached large amplitude. $f = 2.4$ rad s^{-1}; $g_1' = 2.1$ cm s^{-2}; $g_2' = 1.9$ cm s^{-2}; $H_{2M} = 15.2$ cm; $H_{3M} = 12.7$ cm; and $Q = 4.1$ cm^3 s^{-2}.

When $\epsilon = 1$, the slopes of the two interfaces were roughly equal (figure 3) and $R_3 \approx R$. For $\epsilon > 1$ (figure 4) the slope of the lower interface was less than that of the upper interface and R_3 was slightly greater than R. In some cases in which $\epsilon > 1$ the upper interface intersected the lower interface, resulting in a vortex with a two-layer stratification in a central region and three layers outside this region (in $r < R$). Intrusions along the interface, instabilities and mixing similar to those occurring at a bottom front (Smeed 1987) were observed when these 'internal fronts' formed.

An approximate measure of the shear across the lower interface relative to the shear across the upper interface is

$$\Delta = \frac{g_2'(H_{3M} - H_3)}{g_1' H_1},$$

where H_1, H_3 and H_{3M} are defined in figure 1. If the flow was geostrophic, Δ would be exactly equal to the average shear across the lower interface divided by that across the upper interface. The centrifugal terms, however, cause Δ to be an overestimate of this quantity. The maximum values of Δ are shown in figure 5 as a function of ϵ. When $\epsilon \ll 1$, $\Delta < 1$, but when $\epsilon \gg 1$, $\Delta > 1$. The ratio Δ is zero when the experiments commence and increases during the experiments, and so the values in figure 5 are determined by the condition of the vortex at the onset of instability; this is discussed further in §5.

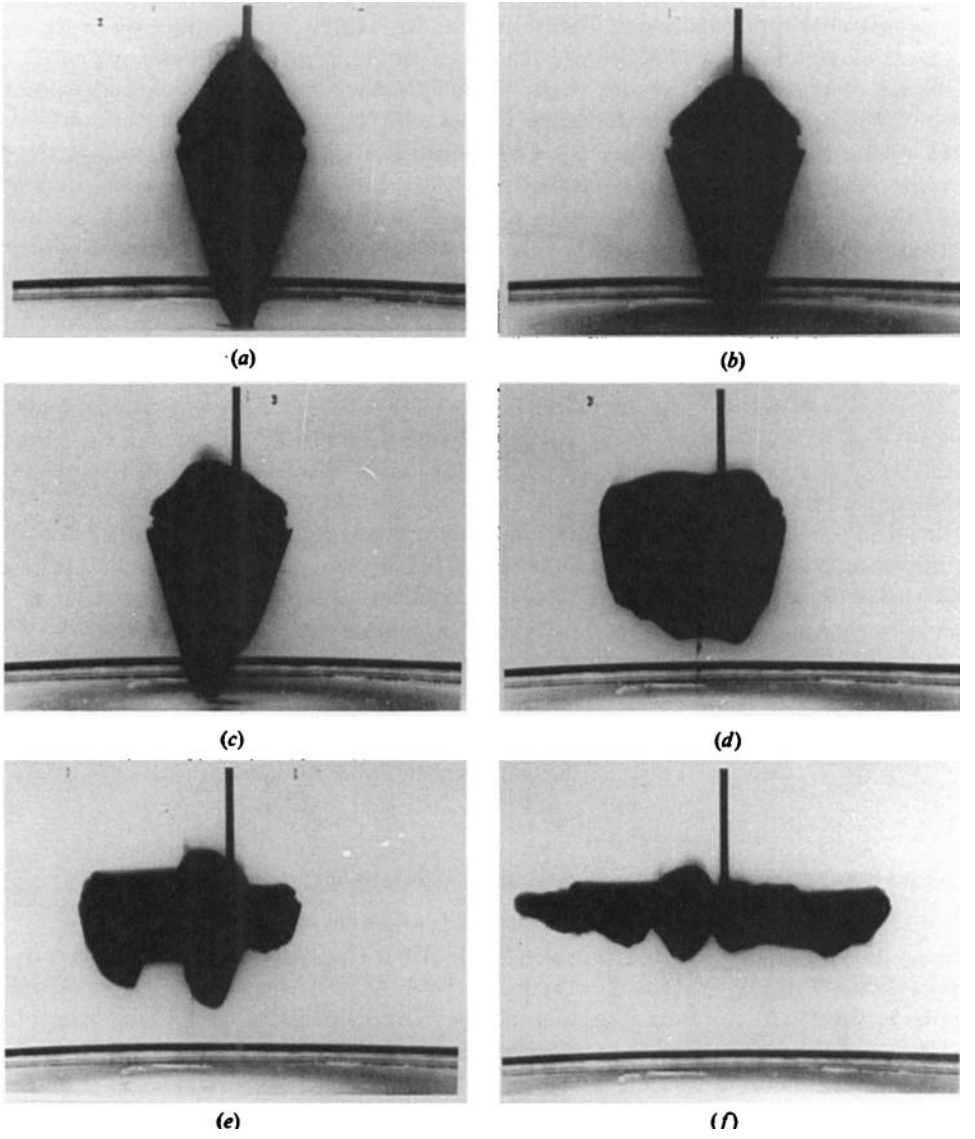

FIGURE 8. 'Intermediate-flux experiment', $\epsilon = 0.43$. (*a*) 106 revs: the vortex is stable and a bottom front has just formed. (*b*) 149 revs: middle-layer fluid has been spread along the bottom in the Ekman layer. (*c*) 161 revs: the source has been turned off and an $N = 1$ disturbance is developing. (*d*) 189 revs: an $N = 2$ instability is also apparent. (*e*) 198 revs: the disturbances have reached large amplitude. (*f*) 238 revs. $f = 2.4$ rad s^{-1}; $g_1' = 0.35$ cm s^{-2}; $g_2' = 0.15$ cm s^{-2}; $H_{2M} = 11.8$ cm; $H_{3M} = 18.4$ cm and $Q = 1.3$ cm^3 s^{-1}.

A measure of the effect of the stratification upon the evolution of the eddy is the change in the rate of increase of depth of the upper layer. The depth of the upper layer in two-layer vortices was found to be of the order of the scale predicted by the inviscid theory of GL

$$\hat{h} = \frac{1}{2}\left(\frac{f^2 Qt}{\pi g'}\right)^{\frac{1}{2}}.$$

There was, though, significant scatter in the data (Smeed 1986). In figure 6 results from a number of three-layer experiments, in which all parameters were kept constant, except for g_2' and H_{2M}/H_{3M} (the total depth $H_{2M}+H_{3M}$ was kept constant) are shown. The results suggest that the lower interface has only a small effect on the depth of the upper layer, but for large values of ϵ the lower stratification causes an increased spreading of the upper layer. This implies that the shear across the upper interface is reduced by the presence of the lower interface, which is to be expected since the middle layer can only be spun-up by the diffuse interfacial Ekman layer, and not by the bottom boundary layer. When $\epsilon \ll 1$, however, the reduction in the spin-up is compensated for by increased stretching of the middle layer.

The evolution of the intermediate-flux vortices was very similar to that of the surface flux eddies, and is illustrated in figures 7 and 8. In these experiments the edge of the eddy was not so well defined and layers are seen at the edge of the eddy (figure 7). These layers are similar to those observed by GL in experiments in which a constant flux of fluid was released in a linearly stratified fluid. GL considered that the layers were a finite-amplitude manifestation of a viscous diffusive overturning proposed by McIntyre (1970).

For an inviscid fluid with infinitely deep upper and lower layers, the shear across the upper and lower interfaces will be equal. However, when the layer depths are finite this will, in general, not be true. An additional asymmetry results from the effect of viscosity. The radial transport in the almost free-stress boundary layer at the upper surface is much less than that in the bottom boundary layer and so the lower layer is spun-up on a much shorter timescale. As a consequence of this asymmetry bottom fronts were formed in some experiments when the lower interface intersected the horizontal boundary (figure 8), but surface fronts were never observed.

4. Axisymmetric behaviour of constant-volume vortices

The adjustment of the surface-volume eddies is very similar to that of two-layer vortices described by GL and Smeed (1986). After the barrier is released the upper layer spreads radially outwards. Within a time $O(f^{-1})$ the spreading is halted as Coriolis and centrifugal forces balance the horizontal pressure gradients. Analytical solutions for the final steady state conserving potential vorticity may be obtained for a related problem in which the flow is two-dimensional rather than axisymmetric. The solutions are determined assuming the conservation of potential vorticity in each layer and a geostrophic balance across each interface. Two examples of the computed interface profiles are shown in figure 9. The lower interface is depressed under the front but raised under the rest of the upper interface. The change in height of the lower interface is always less than that of the upper interface – even when $\epsilon \ll 1$ – and when $\epsilon = O(1)$ it is much less than that of the upper layer.

The effect of the lower interface on the spreading of the upper layer is small. The displacement of the front was measured in a number of experiments and found to be of the order of 1.5 to 2.0 times the deformation radius $(g_1' H_1)^{\frac{1}{2}} f^{-1}$, which is comparable with the displacement of the two-layer vortices.

The adjustment of intermediate-volume vortices is similar to that of the surface-volume eddies. For the special case of infinitely deep upper and lower layers, a simple analytical solution can be found for the steady state conserving potential vorticity for the related two-dimensional problem. The slope of the upper interface is ϵ times

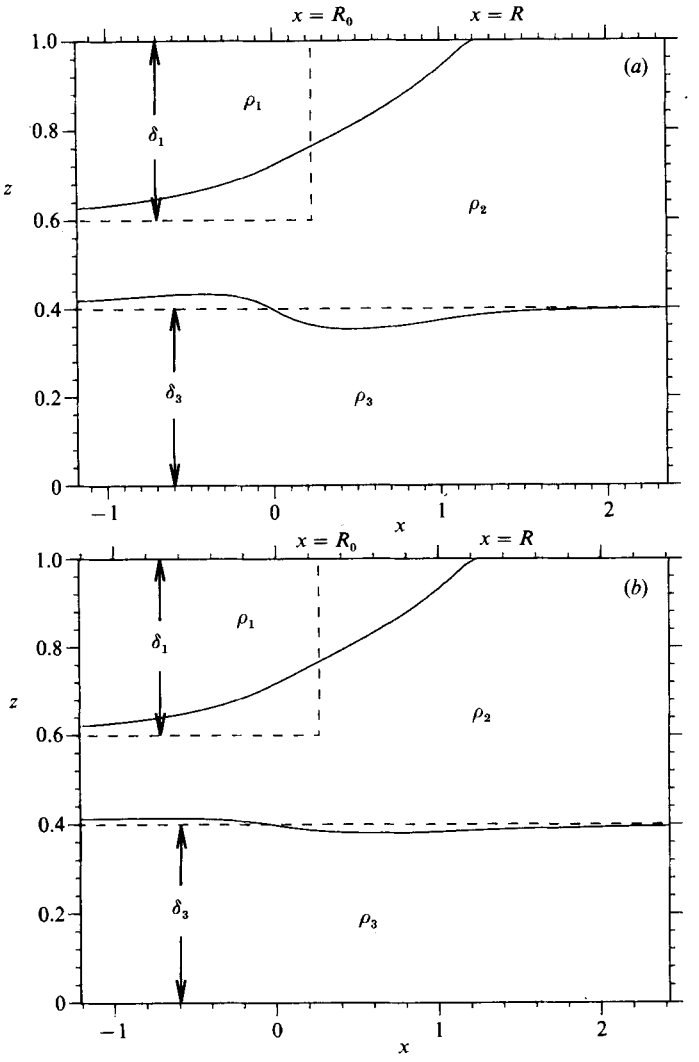

FIGURE 9. Three-layer two-dimensional adjustment. The initial motionless state is shown by the dashed lines. The solid line is the geostrophic solution conserving potential vorticity. The horizontal scale is non-dimensionalized by $(g_1' H_1)^{\frac{1}{2}} f^{-1}$. The surface front is displaced from $x = R_0$ to $x = R$. (*a*) $\epsilon = 0.2$; (*b*) $\epsilon = 0.9$.

that of the lower interface, and the solution is the same as that for the two-layer problem with an infinitely deep lower layer, but with g' replaced by

$$\bar{g} = \left(\frac{1}{g_1'} + \frac{1}{g_2'}\right)^{-1}$$

(i.e. the depth of the middle layer is given by

$$h_2 = H_2\left[1 - \exp\left(\frac{-xf}{(\bar{g}H_2)^{\frac{1}{2}}}\right)\right], \quad x > 0. \tag{4}$$

However, if the system is not initially in the minimum-energy configuration, the whole of the middle layer may be raised or lowered during the adjustment thus releasing large amounts of energy. In the experiments large axisymmetric oscillations which decayed within a few rotation periods were sometimes observed when the vortices were not initially in the minimum-energy configuration. The minimum-energy configuration is given by

$$\frac{H_{1M}-H_1}{H_2} = \frac{g_2'}{g_1'+g_2'}. \tag{5}$$

The displacement of the front, measured approximately one rotation period after the start of the experiment, was usually 1.5 to 2 times the Rossby radius $(\bar{g}H_2)^{\frac{1}{2}}f^{-1}$.

5. The stability of constant-flux vortices

5.1. *Onset of instability – surface-flux experiments*

Non-axisymmetric disturbances with azimuthal wavenumber $N = 1$ or 2 were observed in the two-layer vortices and have been described by GL and Smeed (1986). Perturbations with $N = 2$ were found to be responsible for the largest transfer of energy from the axisymmetric flow to the unstable disturbances, and the discussion of the necessary conditions for the onset of instability was limited to these disturbances. Similarly in this paper 'onset of instability' refers to the appearance of growing instabilities with $N = 2$ that attained large amplitudes.

Smeed (1986) found that the two-layer vortices became unstable when the Froude number, γ (see (1) and (3)), exceeded a critical value γ^*. The value of γ^* was found to be dependent upon λ, a measure of the vertical shear relative to the horizontal shear defined in (2). As λ was decreased γ^* increased. This result was interpreted as the gradient of relative vorticity reducing the gradient of potential vorticity within the lower layer at smaller values of λ, thus stabilizing the vortex. It was also noted that Ekman dissipation can have a significant effect upon the marginally stable state but did not appear to be important in determining the value of γ^* in the range of parameters examined. Thus in order to emphasize the effects of the second interface, values of γ_3^*/γ_2^* are presented here, where

$$\gamma_3^* = \frac{f^2R^2}{g_1'H[\delta_1(1-\delta_1)]^{\frac{1}{2}}}$$

at the onset of instability and γ_2^* is the value of γ^* in the two-layer experiment equivalent to the three-layer experiment but with $g_2' = 0$.

In S1 it was shown that, for quasi-geostrophic flow in a channel, the presence of a second interface could have a significant effect upon the stability of the flow. The stability boundary was found to be a function of S, the ratio of the slope of the upper interface to that of the lower interface, and the parameters

$$\epsilon = \frac{g_2'}{g_1'} \quad \delta_1 = \frac{H_1}{H}, \quad \delta_3 = \frac{H_3}{H}. \tag{6}$$

Although there is a small time required for the instability to reach the amplitude at which it is observed, it is reasonable to assume that the measured values of S, ϵ, δ_1 and δ_3 are close to those at the transition from a stable to an unstable state. If the theory in S1 models the experiments we would expect there to be a correspondence

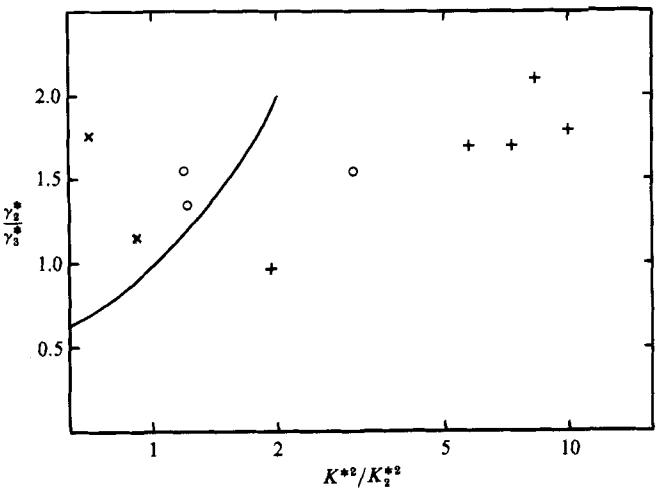

FIGURE 10. The measured values of γ_2^*/γ_3^* *vs.* K^{*2}/K_2^{*2} in the surface-flux experiments. +, $\epsilon < 1$; ×, $\epsilon = 1$; ○, $\epsilon > 1$. The solid line is given by $\gamma_2^*/\gamma_3^* = K^{*2}/K_2^{*2}$.

between this experimentally measured stability boundary and that calculated by the theory. To examine whether this is so the measurements of γ_2^*/γ_3^* are compared (figure 10) with the calculated values K^{*2}/K_2^{*2} where K^* is the largest unstable wavenumber for the measured values S, ϵ, δ_1 and δ_3, and K_2^* is the largest unstable wavenumber in the two-layer flow equivalent to the three-layer flow but with $S = \epsilon = 0$.

When making this comparison, it should be noted that the stability of the two-layer vortices was found to be dependent on parameters other than the Froude number. Similarly it may be expected that γ_3^* is dependent upon parameters (related to features of the flow, such as relative vorticity, which are neglected in the quasi-geostrophic model) other than (6). Furthermore, these parameters may be affected by stratification and thus have values different from those in the two-layer experiment in which γ_2^* was measured.

In the experiments S is defined to be

$$S = \frac{H_{3M} - H_3}{H_1}.$$

The definitions of S and the parameters in (6) were chosen so as to be consistent with the analysis of the two-layer vortices though other definitions are also possible. The amplitude of the $N = 2$ oscillations (as measured by the eccentricity) was greatest near the vortex axis (Smeed 1986), suggesting that H_2 and H_3 are the most appropriate values of the middle- and lower-layer depths. However, a comparison was also made with the results obtained by replacing H_2 and H_3 with H_{2M} and H_{3M} in (6). The results were qualitatively similar indicating that the conclusions are not very sensitive to the definitions of the layer depths used in (6).

Experiments with $\epsilon < 1$

When $\epsilon < 1$ the Rossby radius associated with the lower interface, $\mathscr{R}_3$, is smaller than $\mathscr{R}_1$ (the Rossby radius of the upper interface). The results of the linear stability analysis suggest that for $S > 1$ the lower interface may destabilize the eddy when $R \approx \mathscr{R}_3$ so that $\gamma_3^* < \gamma_2^*$. Such instabilities would be expected to have an amplitude on the upper interface $O(\epsilon)$ times the amplitude on the lower interface. The

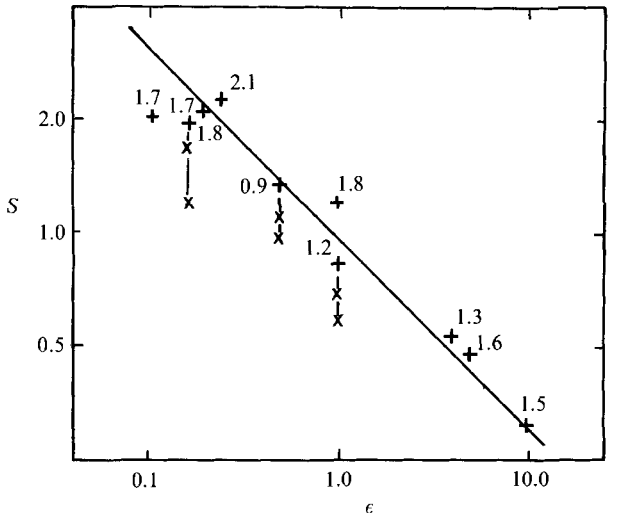

FIGURE 11. Surface-flux experiments. The value of S at the onset of instability as a function of ϵ. The numbers indicate the values of γ_2^*/γ_3^*. The values of S before the onset of instability are shown for some experiments ($\times$). The straight line is given by $S = \epsilon^{-\frac{1}{2}}$.

measurements (figure 10) indicate that $\gamma_2^*/\gamma_3^* > 1$ but is not as large as K^{*2}/K_2^{*2}. There are several possible explanations for this discrepancy.

(i) The short-scale instability is primarily associated with the lower interface and the measurements (figure 5) indicate that when $\epsilon < 1$ the shear across the lower interface is much smaller than that across the upper interface, so that $\lambda_2 \ll \lambda_1$, where

$$\lambda_1 = \left(\frac{g_1' H_1}{fR}\right) \Big/ (\tfrac{1}{2} f R_\nu), \quad \lambda_2 = \left(\frac{g_2'(H_{3M} - H_3)}{fR}\right) \Big/ (\tfrac{1}{2} f R_\nu)$$

($\lambda_1(\lambda_2)$ is a measure of the mean shear across the upper (lower) interface relative to the mean horizontal shear). Note that $\lambda_2/\lambda_1 = \Delta$. The dependence of γ^* upon λ in the two-layer experiments (Smeed 1986) would suggest an increase in γ_3^* sufficient to account for the discrepancy between γ_2^*/γ_3^* and K^{*2}/K_2^{*2}.

(ii) The stability analysis (of inviscid flow) indicated that the growth rates of the short waves were $O(S\epsilon^{\frac{1}{2}})$. During the experiments the values of S increases and it is possible that the vortices become unstable only when $S\epsilon^{\frac{1}{2}}$ attains a sufficiently large value to overcome damping due to dissipation. Measurements (figure 11) indicate that at the onset of stability S was of the order of $\epsilon^{-\frac{1}{2}}$.

(iii) The width of the slope of the lower interface is less than that of the upper, thus reducing the values of the appropriate Froude numbers. This could increase γ_2^*/γ_3^* by 50% but this is not enough to account for the discrepancy in figure 10.

(iv) In some experiments the minimum depth of the lower layer was small at the time of the onset of instability and it is possible that damping due to Ekman dissipation was significantly greater.

It would appear that both (i) and (ii) are important in determining the value of γ_3^* but it is difficult to quantify their relative importance.

In §3 it was noted that in a number of experiments with $\epsilon < 1$ the lower interface intersected the bottom, forming a front. The results of these experiments have been excluded from the discussion so far, but in each of them (five in all) $\gamma_2^*/\gamma_3^* = 1 \pm 0.1$ indicating that the lower interface had no effect upon the instability. This is to be

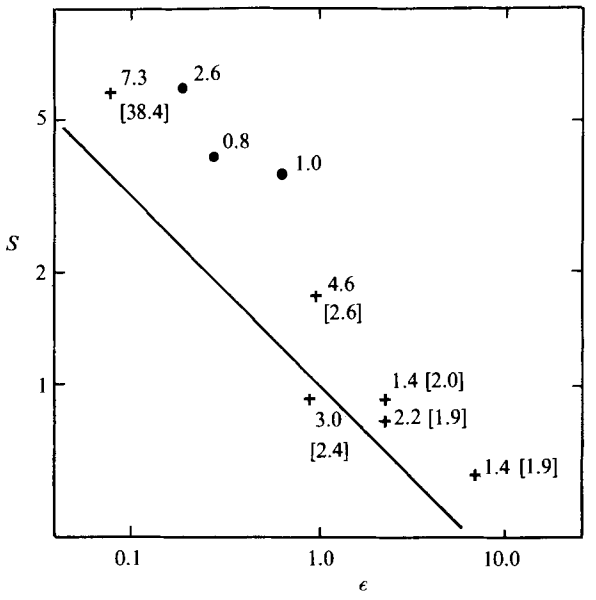

FIGURE 12. Intermediate-flux experiments. The value of S at the onset of instability as a function of ϵ. The numbers indicate the values of γ_2^*/γ_3^* and (in brackets) K^{*2}/K_2^{*2} calculated by the stability analysis. Experiments in which bottom fronts were formed are indicated by circles (●). The straight line is given by $S = \epsilon^{-\frac{1}{2}}$.

expected, since the formation of the front greatly reduces the width of the region over which the lower layer slopes, and in the core of the vortex (where the amplitude of $N = 2$ disturbances is greatest) there is only a two-layer stratification.

Experiments with $\epsilon > 1$

When $\epsilon > 1$ and $S < 1$ then the results of the instability analysis indicate that $\gamma_3^* < \gamma_2^*$, because the instability is primarily an interaction between the upper two layers. The results (figure 10) indicate that $\gamma_3^* < \gamma_2^*$ in these experiments but usually $\gamma_2^*/\gamma_3^* > K^{*2}/K_2^{*2}$. There are several possible explanations for this discrepancy.

(i) The effect of the barotropic velocity. In §3 it was shown that for $\epsilon > 1$ the shear across the upper interface is reduced, suggesting that λ_1 is decreased; this would, though, tend to increase γ_3^* and cannot be responsible for the high values of γ_2^*/γ_3^* (assuming that the instability is primarily associated with the upper interface).

(ii) The width of the sloping region of the lower interface is greater than that of the upper. If this lengthscale was used to calculate γ_3^* then it would be increased by $O(30\,\%)$. This should be sufficient to account for the discrepancies, but it seems unlikely that this would be important if the instability is primarily associated with the upper interface.

(iii) Because the lower interface is slightly diffuse, the effect of Ekman dissipation upon the instabilities in the upper two layers will be reduced. Although this has not been quantified, it seems to be the most plausible explanation for the small ($O(30\,\%)$) differences between γ_2^*/γ_3^* and K^{*2}/K_2^{*2}.

5.2. *Onset of instability – intermediate-flux experiments*

It is not as easy to make a comparison between the experiments with intermediate sources and the theory since the choice of γ_2^* is not as straightforward as for the

surface-flux vortices. However, a value of γ_2^* close to the minimum found in the two-layer experiments was chosen and the values of γ_2^*/γ_3^* were compared with the calculated values of K^{*2}/K_2^{*2} (figure 12). The results demonstrate that in these experiments, in which the interfaces slope in opposite directions, instabilities on scales much shorter than those found in §5.1 are possible. For experiments in which no bottom front was formed the results are qualitatively in agreement with the predicted results. The formation of bottom fronts does, though, have a stabilizing effect upon the eddies. In the three experiments in which fronts were formed γ_3^* was of the order of γ_2^*. Note that the source was turned off before the onset of instability when bottom fronts formed (in all the other intermediate-flux experiments the source was maintained throughout the experiment).

5.3. *Qualitative features of the instabilities – surface-flux experiments*

In figures 2, 3 and 4 experiments are illustrated in which f, Q, g' and H are approximately the same. The value of ϵ, though, is varied thus illustrating the effects of the lower interface on the instability.

The development of an instability with $N = 2$ for $\epsilon = 0.25$ is shown in figure 2; this illustrates the features observed in experiments with $\epsilon < 1$. Before the onset of instability (*a*) the eddy is almost axisymmetric. In this particular example, a small bottom front has formed close to the axis of rotation, but this has very little effect upon the growth of the disturbance. Note that the slope of the lower layer is greater than that of the upper interface. The first signs of instability develop on both interfaces (*b*), and grow to large amplitudes within a few rotation periods (*c*). The perturbations to the upper interface have a scale of the order of the radius of the eddy and are very similar to those seen in two-layer experiments. When viewed in planform the disturbances in the upper layer also appear to develop in the same way as in the two-layer vortices. The eddy becomes elliptical in shape and two arms of upper-layer fluid are drawn out from the core, sometimes leading to splitting of the vortex. A cross-sectioned view in the plane of the major axes of the eddy (*d*) shows disturbances on the lower interfaces of the same scale and a slightly larger amplitude. However, at a later time, in the plane of the minor axes, small-scale perturbations can be seen on the lower interface. They are also evident on the upper interface but their scale is much smaller there. In none of the experiments were such perturbations observed before the onset of the $N = 2$ instability.

In many experiments the eddy restabilized (*f*) becoming almost axisymmetric, before becoming unstable again (*g*). This process occurred as many as three times before the vortex finally broke up (*h*) or the experiment was ended.

In figure 3 an example of a vortex with $\epsilon = 1$ is illustrated. The perturbations to the upper interface do not appear to differ in any significant way from those in the two-layer experiments. Disturbances to the height of the lower layer are of the same order as those on the upper interface and have the same radial structure. There is, however a small difference in phase between the two interfaces, as is expected for baroclinic instabilities that release energy from the mean state.

When $\epsilon > 1$ the Rossby radius associated with the lower interface is greater than that associated with the upper layers. Disturbances to the upper interface are again very similar to those observed in the two-layer experiments, but the radial displacements of fluid elements were greater (figure 4*c*). This was particularly evident from observations of the 'arms' of fluid that spiral outwards from the elliptical upper layer. Perturbations on the lower interface had a smaller amplitude.

5.4. *Qualitative features of the instabilities – intermediate-flux experiments*

Instabilities with $N = 1$ appeared to be more pronounced in these eddies. Sometimes they were seen as a radial displacement of the middle layer (figure 7*c*) or as a bulging of the interface (figure 7*b*). The $N = 2$ perturbations were, as for the surface vortices, the most significant mode of transfer from the mean flow. The development of the $N = 2$ instability is very similar to that in the experiments with surface sources. The eddy first becomes elliptical (figure 7*c*), then arms of middle-layer fluid spiral cyclonically outwards from the vortex (figure 7*d*). Vortices were often observed to restabilize before becoming unstable again at a later time. In none of the experiments was a vortex observed to split completely into two, as happened with many of the surfaces vortices. When the density differences across the upper and lower interfaces were similar ($\epsilon = 1$), the amplitude of the perturbations to the upper and lower layers were very similar (figure 7). In cases in which $\epsilon < 1$ ($\epsilon > 1$), the amplitude of the oscillations was greater (smaller) on the lower interface (figure 8). As the $N = 2$ instability reached large amplitudes, smaller-scale disturbances were observed (figure 8*f*), like those seen in the two-layer experiments. These may be further baroclinic instabilities resulting from the increase in lengthscale or Kelvin–Helmholtz-type instabilities.

6. The stability of constant-volume vortices

6.1. *The initial mode of instability*

In the constant-flux experiments the vortices evolve from a stable to an unstable state and the instabilities are those associated with the marginally stable state. In the constant-volume experiments the initial radius is sufficiently large for the vortex to be unstable, and a range of unstable modes are possible. Linear stability analysis assumes that the mode of instability observed is that with the largest initial growth rate. However, when the perturbations are observed their amplitude is no longer small, and nonlinear interactions may result in the observed mode being different from the mode that initially had the largest growth rate.

In both variations of the three-layer experiments baroclinic instabilities very similar to those observed in two-layer vortices were seen to develop within a few ($\lesssim 5$) rotation periods after the start of the experiment. In order to examine the effect of the three-layer stratification upon the initial mode of instability, the wavenumber N of the first observed disturbance was recorded for each experiment and compared with N_2, the wavenumber that would be expected for the equivalent two-layer experiment (i.e. that with $g_2' = 0$). The values of N_2 were taken from GL's figure 5. The results are summarized in figure 13 for the surface-volume vortices. The results of the stability analysis suggest that, because the mean slope of the lower interface is less than that of the upper interface (see figure 9), it will not have a large effect upon the initial growth of instabilities. This appears to be true over the range of parameters explored here.

Results from intermediate-volume experiments are shown in figure 14. The results are scaled both by the wavenumber that would be expected if $g_2' = 0$, plotted as a function of S_0 and ϵ, and by the wavenumber that would be expected if $g_1' = 0$, plotted as a function of $1/S_0$ and $1/\epsilon$ (i.e. there are two points for each experiment). By symmetry we would expect the results to be the same. S_0 is the value of S before adjustment and the value S_1 of S after adjustment will be different. However, if it is the gradients of potential vorticity within each layer that are important rather

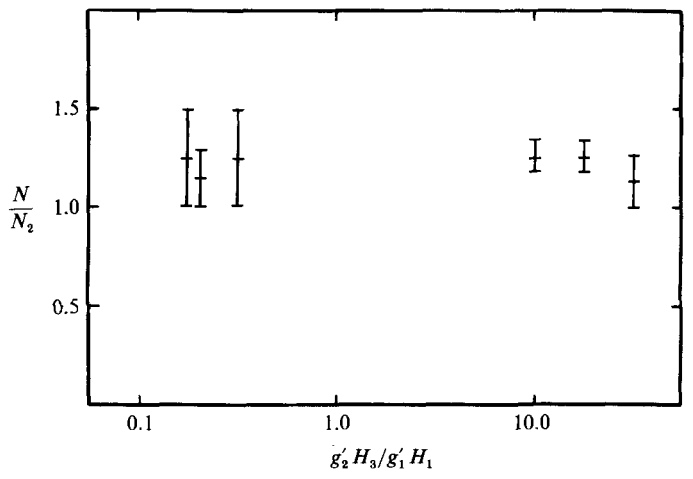

FIGURE 13. The initial wavenumber N observed in the surface-volume experiments as a function of $g_2' H_3/g_1' H_1$. N_2 is the wavenumber expected in the equivalent two-layer experiment with $g_2' = 0$, taken from GL's figure 5.

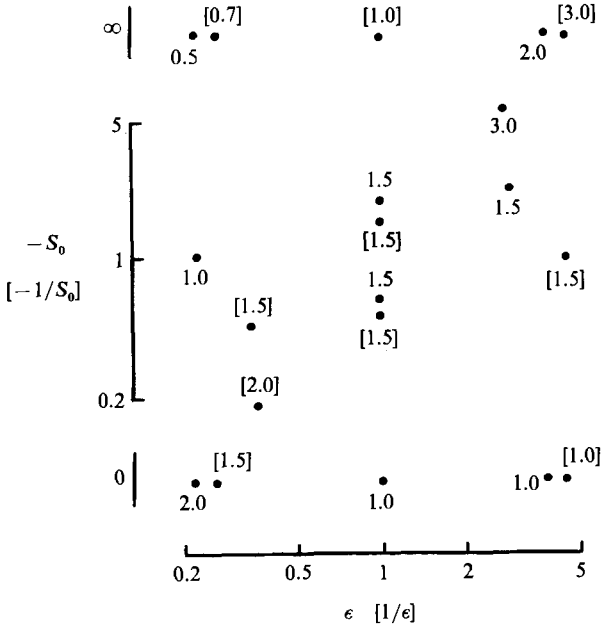

FIGURE 14. The initial wavenumber N observed in the intermediate-volume experiments scaled by N_2 (the wavenumber expected in the equivalent two-layer experiment with $g_2' = 0$, taken from GL's figure 5) as a function of S_0 and ϵ. Also shown (figures in brackets) is N/N_2' (N_2' is the wavenumber expected in the equivalent two-layer experiment with $g_1' = 0$) as a function of $1/S_0$ and $1/\epsilon$.

than just the changes of depth within each layer, than S_0 is more appropriate than S_1. (Note that in the theory in S1 there were no horizontal gradients of velocity and so a gradient in the layer depth was equivalent to a gradient of potential vorticity.) The error bounds for N/N_2 are large because N was often small, and so a quantitative comparison with the theory has not been made. The results do, though, agree

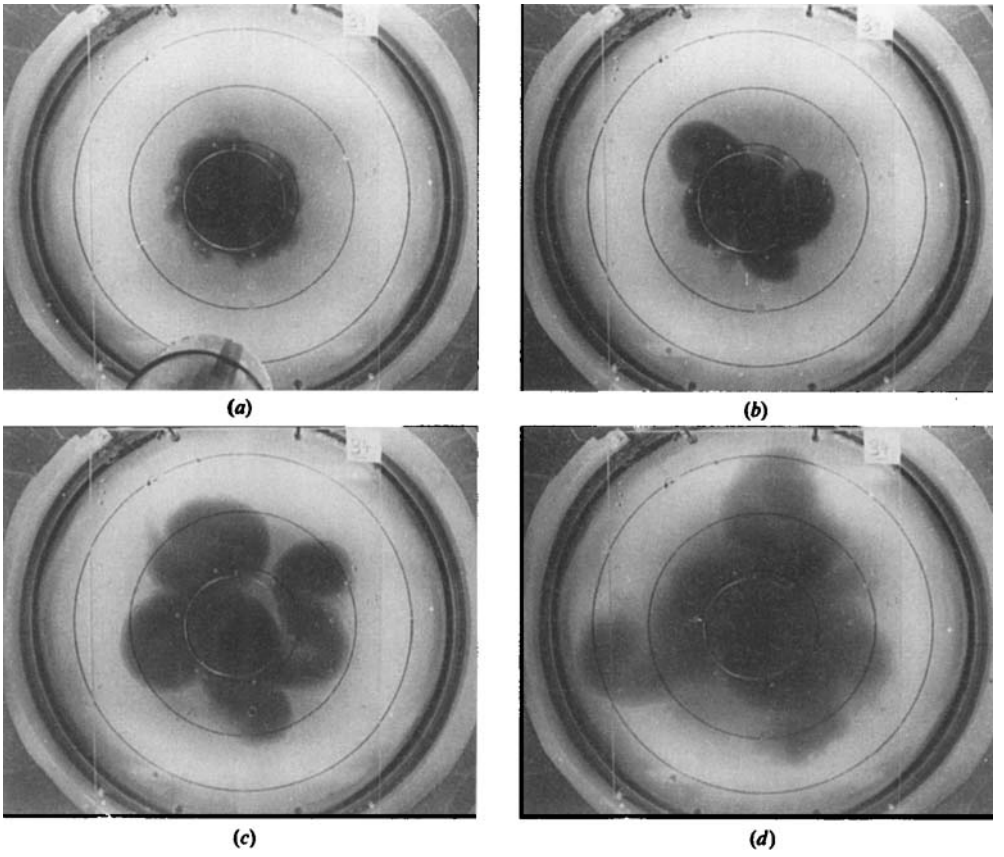

FIGURE 15. Two-layer surface-volume experiment, $\epsilon = 0$. (*a*) 2 revs; (*b*) 6 revs; (*c*) 16 revs; (*d*) 32 revs. $f = 1.67$ rad s^{-1}; $g' = 2.0$ cm s^{-2}; $H_1 = 5.0$ cm; $H_{2M} = 15.0$ cm.

qualitatively very well with the conclusions of the theoretical model. In particular it can be seen that:

(*a*) $\epsilon > 1$. For small S_0 the lower interface acts somewhat like a rigid boundary decreasing the effective depth and so increasing the wavenumber of the instability. But as S_0 increases, the lower interface suppresses the short-scale instabilities and at large S_0 long-wave disturbances are the first to develop.

(*b*) $\epsilon \approx 1$. For $S_0 = O(1)$ shorter-scale waves grow than would be expected in a two-layer system. This is due to the interaction of the two interfaces which slope in opposite directions.

(*c*) $\epsilon < 1$. For $S_0 \ll 1$ the lower interface has no effect but as S_0 is increased, shorter-scale wavelengths associated with the lower interface dominate.

6.2. *Large-amplitude behaviour – surface-volume eddies*

Photographs of two experiments showing instabilities of surface vortices are shown in figures 15 and 16. The first is of a two-layer eddy and the second has a three-layer stratification. The parameters are the same for each experiment except for ϵ: in figure 15 $\epsilon = 0$ and in figure 16 $\epsilon = 5$. The initial wavenumber of the instability is 4 in the two-layer experiment (figure 15*b*) and 5 in the three-layer experiment (figure 16*b*). At later times it can be seen that stronger cyclones are formed in the three-layer

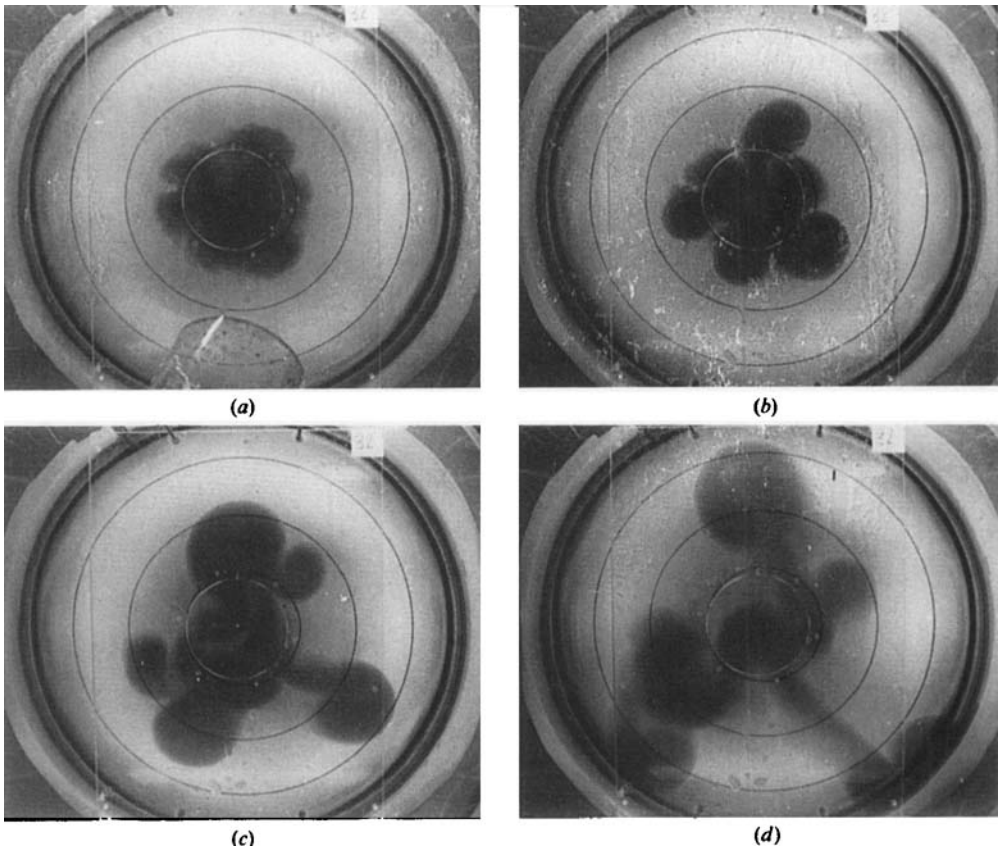

FIGURE 16. Three-layer surface-volume experiment, $\epsilon = 5$. (*a*) 3 revs; (*b*) 6 revs; (*c*) 10 revs; (*d*) 16 revs. $f = 1.67$ rad s^{-1}; $g_1' = 2.0$ cm s^{-2}; $g_2' = 20.0$ cm s^{-2}; $H_1 = 5.0$ cm; $H_{2M} = 10.0$ cm; $H_{3M} = 5.0$ cm.

experiment, resulting in larger radial displacements of the vortex pairs (compare figure 15*c* with 16*d*). The cyclones are stronger in the three-layer eddy because their depth is limited by the lower interface, resulting in greater stretching, and also because the effects of Ekman dissipation are not as large as in the two-layer experiment. It is also apparent in figure 16 that although initially $N = 5$, three anticyclones in the upper layer grow faster than the others. The size of vortices formed in two-layer experiments varied but the variation is much more pronounced in the three-layer flows in which the Rossby radius of the lower layer was much greater than that of the upper layer.

When the Rossby radius of the lower interface was the smaller of the two, observation of the upper layer did not reveal any significant differences from the two-layer experiments. However, the stability analysis indicates that small-scale disturbances with $O(1)$ amplitude on the lower interface will only have small ($O(\epsilon)$) amplitudes on the upper layer and would not be revealed by the method of observation used here. It may, though, be possible that small-scale disturbances are generated similar to those observed in the constant-flux experiments since potential energy of the upper layer is transferred to kinetic energy and potential energy of the lower layer by the large-scale baroclinic instabilities associated with the upper interface.

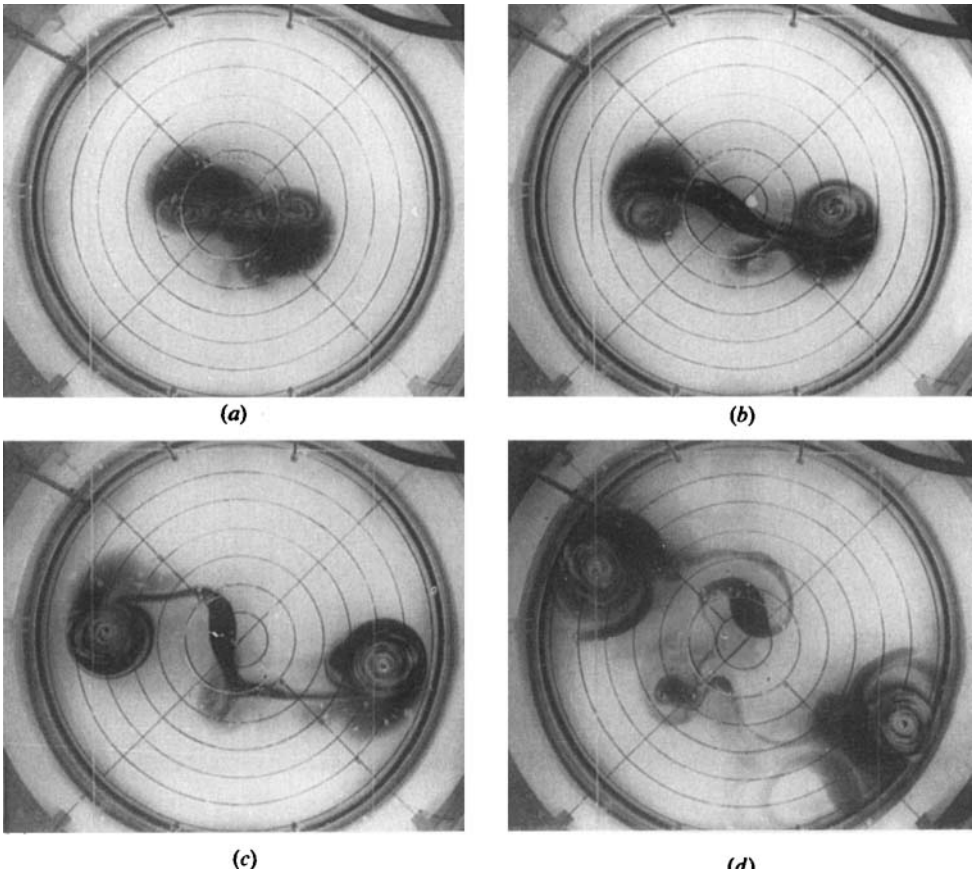

FIGURE 17. Intermediate-volume experiment, $\epsilon = 0.22$, $S_0 = 0$. (*a*) 3 revs; (*b*) 5 revs; (*c*) 8 revs; (*d*) 16 revs. $f = 1.68$ rad s^{-1}; $g_1' = 9.4$ cm s^{-2}; $g_2' = 2.1$ cm s^{-2}; $H_{1M} = 6.8$ cm; $H_2 = 5.2$ cm; $H_{3M} = 7.1$ cm.

6.3. *Large-amplitude behaviour – intermediate-volume vortices*

In §6.1 it was noted that the initial wavenumber was dependent upon S_0 and if the Rossby radii associated with the two interfaces are different, a wide range of values of the azimuthal wavenumber N is possible. Examples of two such experiments are shown in figures 17 and 18. The parameters were the same in each experiment except for S_0. In figure 17 $S_0 = 0$ and in figure 18 $S_0 = \infty$. In both experiments $\epsilon = 0.22$. In figure 17 the initial value of N is 2. Note that it is the middle layer that has been dyed but the streak particles are on the surface of the upper layer. Strong vortex pairs form tearing the eddy apart. The phase shift between the upper two layers is opposite in sign to that in the surface-eddy experiments (figures 15 and 16), but in the present example the interface slope is in the opposite direction. Thus in both cases the phase shift is such as to release energy from the mean flow. The cyclonic vortices in the upper layer are so strong that between figures 17 (*b*) and (17 (*d*) (11 rotation periods), the middle-layer anticyclones more completely around their adjacent cyclones. This indicates that during the adjustment the whole of the middle layer was displaced downwards a significant amount. In contrast, when $S_0 = \infty$ (figure 18), the initial wavenumber of the disturbance is 6; however, some waves appear to grow faster

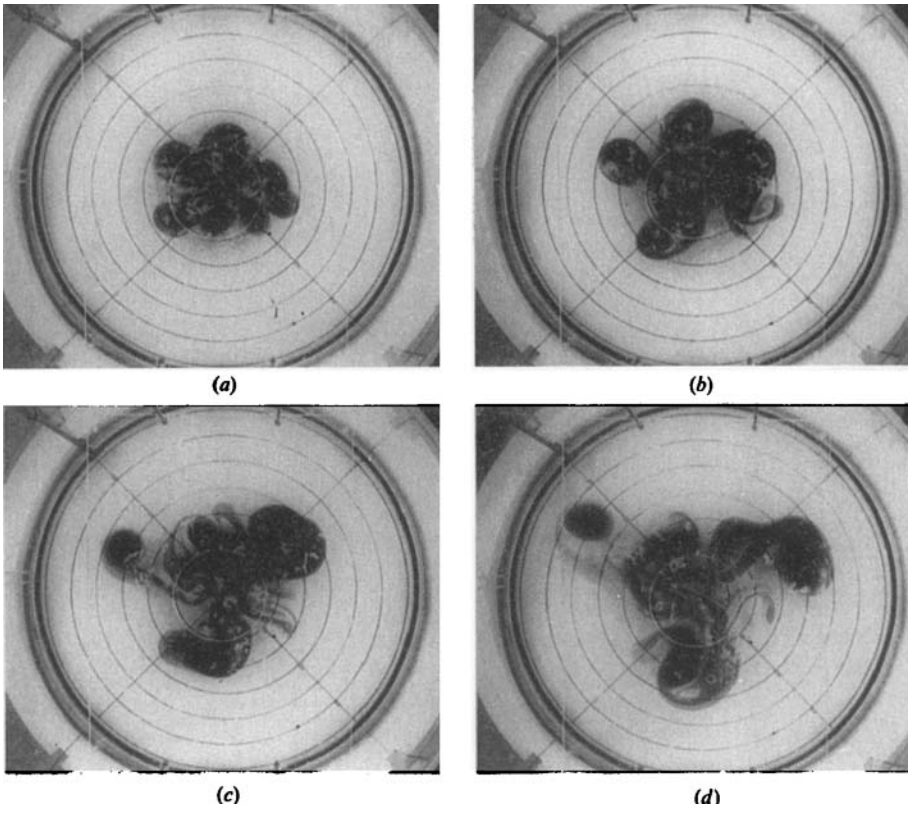

FIGURE 18. Intermediate-volume experiment, $\epsilon = 0.22$, $S_0 = \infty$. (*a*) 3 revs; (*b*) 6 revs; (*c*) 10 revs; (*d*) 16 revs. $f = 1.68$ rad s^{-1}; $g_1' = 9.5\ cm\ s^{-2}$; $g_2' = 2.1$ cm s^{-2}; $H_{1M} = 7.0$ cm; $H_2 = 5.4$ cm; $H_{3M} = 7.1$ cm.

than others and at a later time (figures 18*c* and *d*), the flow is dominated by disturbances with $N = 3$. Vortex pairs also form in this example but the cyclones (in the lower layer) are not as intense as those (in the upper layer) when $S_0 = 0$.

7. Discussion

Griffiths & Pearce (1985) presented some observation of an anticyclonic eddy derived from the Leeuwin current south of Australia. The eddy was elliptical in shape and two arms of warm water spiralled out from its centre. By comparison with the experiments of GL, they suggested that the ring was in the process of splitting as the result of baroclinic instability. Similar features have been observed in Gulf Stream rings. Evans *et al.* (1985) reported an eccentricity of up to 0.3 for ring 82-B, and Joyce & Kennelly (1985) observed strong cyclonic vortices around the periphery of the same ring. Both these features are suggestive of baroclinic instabilities similar to those observed in the experiments.

Smeed (1986) estimated the Froude numbers of some observed eddies. The values were of the same order, though less than, the critical values measured in the experiments with two-layer constant-flux vortices. The conclusions of the present study indicate that stratification below the main thermocline may also be important in determining the critical size required for instability, and other features of the

instability. A number of detailed observations have been made of ring 82-B (Evans *et al.*; Olson *et al.*; Joyce & Kennelly 1985), making it a suitable example to examine.

In April 1982 ring 82-B had a radius of 85 Km and the depth of the thermocline on the axis of the vortex was 570 m. The average total depth was ≈ 2700 m (though there was significant bottom slope). Olson *et al.* (1985) used a correlation between the depth of the 10 °C isotherm and the difference in dynamic height between 100 dbar and 2000 dbar to calculate an effective g_1' of 0.01 m s^{-2} across the thermocline. This gives a value of γ of 5. Across the pycnocline the potential density changes by 0.9 kg m^{-3}; assuming $N = 6 \times 10^{-4}$ rad s^{-1} the potential density increases a further 0.3 kg m^{-3} down to 2700 m. Representing the stratification below the pycnocline by a second interface at a depth midway between the pycnocline and the bottom gives $\epsilon \approx 0.3$, $\delta_1 = 0.2$, $\delta_3 = 0.4$. The eddy is thus comparable with the experiments examined here in which $\epsilon < 1$. Unfortunately potential-density sections at a depth of 1600 m were not presented and so an appropriate value of S cannot be estimated. The results of the present study indicate that the size at which the eddy become unstable will only be affected by the lower stratification if $S > 1$. However, in the experiments small-scale instabilities (associated with the lower stratification) were observed to develop after the onset of the large-scale instability and this may also be the case for warm-core rings.

In S1 the application of three-layer models to flows with more general density profiles was discussed. The normal modes of three-layer flow were calculated and it was suggested that these could model qualitatively the first three modes of a continuous system, but it was shown that the analogy could not be exact since there are only three parameters that can be varied in the layer model, but five constants in the modal equations.

Although only experiments with single eddies have been examined, the results have some implications for the evolution of a field of vortices. Griffiths & Hopfinger (1984) studied the temporal development of turbulence in a two-layer stratified rotating fluid generated by baroclinic instability at a front. They found that after an initial period of adjustment the lengthscale of the turbulent field remained constant in time, in contrast to turbulence in homogeneous rotating fluids in which inertial interactions transfer energy to larger lengthscales. In the two-layer flow, however, baroclinic instability blocked this cascade, by generating eddies on a scale of the order of the Rossby radius. The results of the experiments described here demonstrate that when two or more baroclinic modes are possible, baroclinic instability may generate motion on a variety of scales, and the observations have revealed changes in lengthscale in time as energy is transferred between the two interfaces by baroclinic instabilities (and also by the spin-down process). These observations suggest that turbulence in continuously stratified fluids may differ significantly from that in the two-layer experiments described by Griffiths & Hopfinger (1984).

8. Conclusions

The stability of three-layer stratified axisymmetric vortices has been examined in laboratory experiments and the observations have been interpreted using a linear stability analysis of quasi-geostrophic flow (Smeed 1988).

Experiments with surface-flux vortices showed that the presence of a second interface may destabilize eddies at scales smaller than would otherwise be possible, thus decreasing the critical Froude number γ_3^*. When $\epsilon < 1$ and $S > 1$, instabilities

primarily associated with the lower interface may develop. The decrease in the value of γ_3^* (relative to that which would be expected in the absence of the lower interface) measured in the experiments was not as great as that predicted by the linear theory. Two explanations were proposed. First, that the horizontal gradients of relative vorticity reduced the gradient of potential vorticity in the lower layer, thus tending to stabilize the eddy. Secondly it was noted that the analysis predicts growth rates of order $S\epsilon^{\frac{1}{2}}$ for instabilities associated with the lower interface, so that dissipation may suppress short scale instabilities for $S \lesssim \epsilon^{-\frac{1}{2}}$. Sometime after the initial instability, secondary instabilities with smaller lengthscales were observed. These had $O(1)$ amplitude on the lower interface but were small on the upper interface.

When $\epsilon \gg 1$ and $S < 1$, γ_3^* may also be decreased because the lower interface acts somewhat like a rigid boundary decreasing the depth to which the perturbations penetrate, thus reducing the effective Rossby radius.

Intermediate-flux vortices, in which the two interfaces slope in opposite directions, were found to become unstable at scales significantly shorter than when the interface slopes had the same sign.

Results from experiments with constant-volume vortices showed that the wavenumber of the fastest-growing disturbance was dependent upon S as well as the Froude numbers. The dependence of the initial wavenumber upon the parameters agreed qualitatively well with the results of the simple model of quasi-geostrophic flow described in S1. It was also noted in these experiments that the dominant lengthscale of the flow changed during the course of the experiment, owing to the possibility of baroclinic instability on two different scales. This phenomenon has not been investigated in detail here, but such a study could perhaps be undertaken along the lines of the experiments by Griffiths & Hopfinger (1984), who examined the behaviour of a turbulent field of eddies in a two-layer stratified rotating fluid.

It has been suggested (Griffiths & Pearce 1985; Smeed 1986) that instabilities very similar to those in the experiments described by GL are responsible for the breakup of warm-core rings in the oceans. The results presented here indicate the importance of stratification below the main thermocline when examining the stability of ocean eddies.

I am very grateful to Dr Paul Linden for his guidance and encouragement during the course of this research. I am also grateful to the staff of the DAMTP laboratory, Mr D. Cheesley, Mr D. Lipman and Mr J. Sharpe, for the construction of the apparatus. Financial support from the Natural Environment Research Council is gratefully acknowledged.

REFERENCES

Chia, F., Griffiths, R. W. & Linden, P. F. 1982 Laboratory experiments on fronts. Part II. The formation of cyclonic eddies at upwelling fronts. *Geophys. Astrophys. Fluid Dyn.* **19**, 189–206.

Evans, R. H., Baker, K. S., Brown, O. B. & Smith, R. C. 1985 Chronology of warm-core ring 82-B. *J. Geophys. Res.* **90**, 8803–8811.

Gill, A. E., Smith, J. M., Cleaver, R. P., Hide, R. & Jonas, P. R. 1979 The vortex created by mass transfer between layers of a rotating fluid. *Geophys. Astrophys. Fluid Dyn.* **12**, 195–220.

Griffiths, R. W. & Hopfinger, E. J. 1984 The structure of mesoscale turbulence and horizontal spreading at ocean fronts. *Deep-Sea Res.* **31**, 245–269.

Griffiths, R. W., Killworth,, P. D. & Stern, M. E. 1982 Ageostrophic instability of ocean currents. *J. Fluid Mech.* **117**, 343–377.

GRIFFITHS, R. W. & LINDEN, P. F. 1981*a* The stability of vortices in a rotating, stratified fluid. *J. Fluid Mech.* **105**, 283–316.

GRIFFITHS, R. W. & LINDEN, P. F. 1981*b* The stability of buoyancy driven coastal currents. *Dyn. Atmos. Oceans* **5**, 281–306.

GRIFFITHS, R. W. & LINDEN, P. F. 1982 Laboratory experiments on fronts: Part 1. Density driven boundary currents. *Geophys. Astrophys. Fluid Dyn.* **19**, 159–187.

GRIFFITHS, R. W. & PEARCE, A. F. 1985 Satellite images of an unstable warm core eddy derived from the Leeuwin Current. *Deep-Sea Res.* **32**, 1371–1380.

HART, J. E. 1972 A laboratory study of baroclinic instability. *Geophys. Fluid Dyn.* **3**, 181–209.

JOYCE, T. M. & KENNELLY, M. A. 1985 Upper ocean velocity structure of Gulf Stream warm-core ring 82-B. *J. Geophys. Res.* **90**, 8813–8822.

KILLWORTH, P. D., PALDOR, N. & STERN, M. E. 1984 Wave propagation and growth on a surface front in a two-layer geostrophic current. *J. Mar. Res.* **42**, 761–785.

MCINTYRE, M. E. 1970 Diffusive destabilisation of the baroclinic circular vortex. *Geophys. Fluid Dyn.* **1**, 19–57.

OLSON, D. B., SCHMITT, R. W., KENNELLY, M. A. & JOYCE, T. M. 1985 A two-layer diagnostic model of the long-term evolution of warm-core ring 82-B. *J. Geophys. Res.* **90**, 8813–8822.

PHILLIPS, N. A. 1954 Energy transformation and meridional circulation associated with simple baroclinic waves in a two-level, quasi-geostrophic model. *Tellus* **6**, 273–286.

SAUNDERS, P. M. 1973 The instability of a baroclinic vortex. *J. Phys. Oceanogr.* **3**, 61–65.

SMEED, D. A. 1986 Eddies in stratified, rotating fluids. Ph.D. thesis, University of Cambridge.

SMEED, D. A. 1987 A laboratory model of benthic fronts. *Deep-Sea Res.* **34**, 1431–1459.

SMEED, D. A. 1988 Baroclinic instability of three-layer flows. Part 1. Linear stability. *J. Fluid Mech.* **194**, 217–231.